This is the author-manuscript version of this work - accessed from
http://eprints.qut.edu.au

Mahendran, Mahen (2007) Applications of finite element analysis in structural engineering. In Siva Prasad, N. and Sekar, A.S. and Krishnapillai, S., Eds. *Proceedings International Conference on Computer Aided Engineering*, pages pp. 38-46, Chennai, India.

Copyright 2007 (please consult author)

Applications of Finite Element Analysis in Structural Engineering

M. Mahendran
Faculty of Built Environment and Engineering, Queensland University of Technology, Australia
Fax: +61 7 3138 1170, E-mail: m.mahendran@qut.edu.au

Abstract

Advances in the field of computer aided engineering during the last two decades have been quite extensive and have led to considerable benefits to many engineering industries. In the building industry, use of advanced finite element tools has not only allowed the introduction of innovative and efficient building products, but also the development of accurate design methods. High performance computing facilities and advanced finite element programs are now available for research and development activities in many universities in collaboration with industries. In this paper, four examples of successful applications of advanced computer tools are presented and discussed. The structural performance of steel cladding systems, innovative hollow flange beams, plasterboard lined cold-formed steel stud walls and an innovative cold-formed steel building system was accurately simulated by finite element models and thus considerably reduced the number of time consuming and expensive large scale experiments required. Both local and overall failures of various building components were investigated. New design rules, structurally improved and optimized building products and systems, and simplified behavioural and computer models were developed. This paper presents a summary of the four detailed investigations using advanced finite element tools, and selected results.

Keywords: *Finite element analysis, Structural engineering, Building industry*

1. Introduction

Traditionally, engineers have used laboratory testing to investigate the structural behaviour of steel building products and systems subject to the expected wind and earthquake loads and to develop appropriate design rules. Laboratory testing was also used to develop new building products and systems. However, such reliance on time consuming and expensive laboratory testing has hindered progress in this area. The product manufacturers and designers often decided on conservative designs in order to avoid expensive and time consuming laboratory testing. However, advances in the field of computer aided engineering during the last two decades have changed this situation significantly in many engineering industries. In the building industry, the use of advanced finite element tools has not only allowed the introduction of innovative and efficient building products, but also the development of accurate design methods. During the last decade, Queensland University of Technology researchers have undertaken many collaborative research projects with their industry partners using advanced computing facilities and finite element tools, resulting in considerable benefits to the industries. In this paper, four examples of successful applications of advanced computer tools are presented and discussed. These examples were steel cladding systems, innovative hollow flange beams, plasterboard lined cold-formed steel stud walls, and an innovative cold-formed steel building system.

2. Steel Roof and Wall Cladding Systems

Australian steel claddings are made of very thin and high strength steel (0.42 mm G550 steel with 550 MPa yield

strength), and are crest-fixed with screw fasteners. Figure 1 shows one of the commonly used profile. These claddings often suffer from local pull-through failures at their screw connections under wind uplift/suction loading caused by storms and cyclones [1,2]. The presence of large stress concentrations in the crest-fixed sheeting around the fastener holes is attributed to these local failures in which the screw heads pull through the sheeting (Fig.2a). These failures are initiated by a transverse splitting at the fastener holes [1,3], and lead to rapid loss of the entire roof and significant building damage. For some steel claddings, a local dimpling failure also occurs without any splitting (Fig.2b). Current design formulae for the strength of screwed connections in tension were found to be inadequate to predict the local failure strength of connections in these cladding systems [3]. Hence cladding manufacturers rely on expensive and time consuming testing methods. To overcome this problem, a thorough investigation based on extensive finite element analyses was carried out.

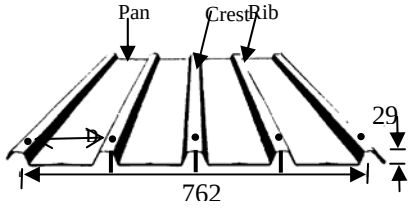

(a) Trapezoidal roofing –wide pans

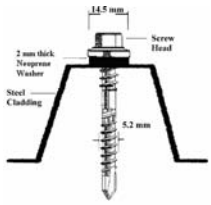

(b) Crest-fixing

Figure 1. Crest-fixed Profiled Steel Cladding

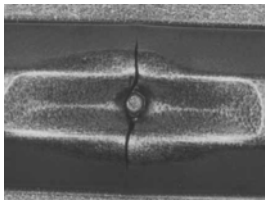

(a) Pull-through failure

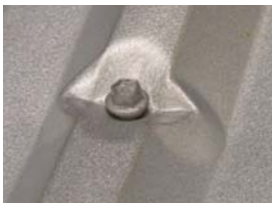

(b) Dimpling failure

Figure 2. Local Failures

2.1 Model Description and Validation

A two-span trapezoidal cladding assembly with simply supported ends was considered adequate in representing multi-span assemblies. In this study, a half width model with one span and appropriate boundary conditions was analysed using a finite element program ABAQUS [4]. Shell elements (S4R5) were used to model both the in-plane membrane and bending actions in the sheeting, large cross-sectional distortions, localised yielding and deformations around the fastener holes, and both geometric and material nonlinearities. Three dimensional eight noded continuum elements were used to model the screw head. The hyperelastic behaviour of neoprene washer located between the screw head and sheeting was modelled by using ABAQUS hybrid elements, C3D8H eight noded continuum elements. Master slave contact pair option was used to model neoprene washer between the screw head and sheeting. Figure 3 shows the details of the finite element model used. A uniform surface pressure across all shell elements simulated the static wind uplift pressure loading adequately. Nonlinear analyses were undertaken by including geometry and material effects and a fracture criterion that was developed from experiments and included using ABAQUS USER SUBROUTINES option.

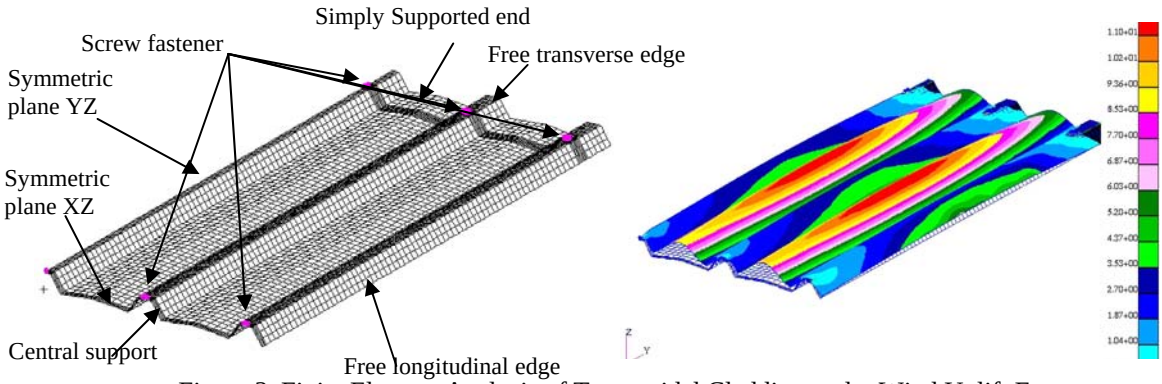

Figure 3. Finite Element Analysis of Trapezoidal Cladding under Wind Uplift Forces

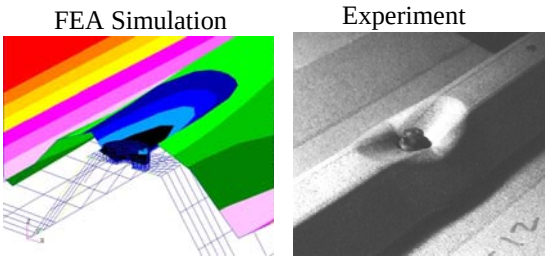

Figure 4. Simulation of Local Failures

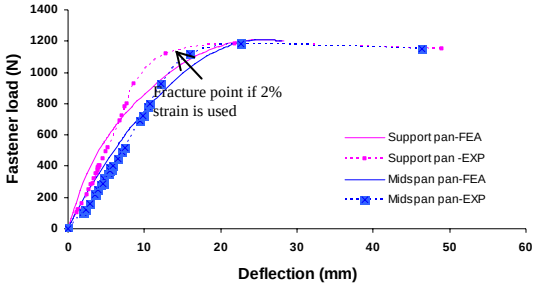

Figure 5. Comparison of Load-deflection Curves

The chosen finite element model was validated by comparing its results with corresponding experimental results of deformation shapes (cross-sectional distortion in Fig.3, local dimpling of crests and high stress concentrations including longitudinal membrane action and yielding around the fastener holes in Fig.4), pull-through and dimpling failure loads and load-deflection curves (Fig.5). The improved finite element model with splitting criterion was able to model the local pull-through failures in the less ductile G550 steel claddings that are initiated by transverse splitting at the fastener hole.

2.2 Parametric Study and Design Rules

The validated finite element model was then used to determine the local pull-through and dimpling failure loads of a range of trapezoidal steel claddings (728 cases). The following important parameters were varied in this study. Steel thickness t; yield stress f_y; Young's modulus E; diameter of screw head or washer d; crest width w_c; crest height h_c; pitch p; pan height h_p; trough width w_t; and span L. The results were grouped and analysed to develop a non-dimensionalised strength formula that predicts the fastener failure load ($F_{ov,}$). Further details of FEA and results are available in [5].

Trapezoidal claddings with wide pans

$$F_{ov} = 0.04\left(8.5-\frac{30 f_y d}{Et}\right)^2\left(\frac{h_c}{p}\right)^{3/4}\left(\frac{w_t}{w_c}\right)^{1/5}\left(0.9+\frac{1400t^2}{Ld}\right)^{1/3} dtf_y \quad (1)$$

The pull-through/local dimpling failure load can be reliably predicted using Eq. (1) with a ϕ factor of 0.5 within the current provisions of AS/NZS 4600 [6]. A similar approach was used for other two commonly used profiles, Trapezoidal sheeting with closely spaced ribs and corrugated sheeting, and the required design rules were developed [7].

3. Cold-formed Steel Stud Wall Systems

Gypsum plasterboard is a common lining material for steel wall frame systems, and is used in combination with cold-formed steel studs (unlipped or lipped C-sections) for both the load bearing and non-load bearing walls in the residential, industrial and commercial building construction. Since plasterboard is not considered as a structural material, considerable strengthening effects of the plasterboard in carrying axial (or other) loads are simply ignored. Therefore a detailed investigation based on finite element modeling and experiments of both sides lined stud walls was undertaken.

3.1 Model Description and Validation

The cold-formed steel wall frames used in the experimental study [8] were first used in the finite element analyses (see Table 1). They were made of three cold-formed unlipped C-section studs and two tracks (Fig.6). The studs were connected to the top and bottom tracks using a 8-18x12 mm wafer head screw at each joint. The wall frames were lined on both sides with 10 mm plasterboard using Type S 8-18x30 mm plasterboard screws at 220 mm centres. There were two C-sections, two steel grades and two stud spacings of 300 and 600 mm, giving a total of eight wall frames.

Table 1. Details of Stud Wall Frames and their Ultimate Loads for 600 mm Stud Spacing

Frame	Stud Size (mm)			Steel Grade	Ultimate Loads of Studs (kN)		$\frac{FEA}{Expt.}$
	Web (D)	Flange (b)	t		FEA	Experiments	

1	75	30	1.15	G2	17.5	21.2, 22.2, 20.6	0.825, 0.788, 0.849
2	75	30	1.20	G500	34.4	35.3, 35.3, 36.5	0.975, 0.975, 0.942
3	200	35	1.15	G2	21.9	22.0	0.995
4	200	35	1.20	G500	34.5	41.5, 41.5, 42.2	0.831, 0.831, 0.883

Figure 7 shows the finite element model of unlined and lined stud walls based on the top half of the stud and the top track. The track and the steel studs were modeled using ABAQUS S4R5 shell elements [4]. At the top track to stud connection, the screws were modelled as beam elements (B31 elements). A rigid body R3D4 element was used to model the steel sheets between the track and the stud. For these elements the reference node adopted was the node at the top of the track in which the load was applied. These elements were used to transfer the axial load to the entire stud area without any rotational restraint. Two additional elements were required to complete the model for both sides lined frames. They were the screws connecting the plasterboard to the studs, modelled as B31 beam elements, and the 10 mm plasterboard on both sides, modeled as S4R5 elements. Since the top end of the stud was not rigidly connected to the underside of the track webs, the rigid body nodes and the elements in the track web were modelled as contact pairs. The flanges of the track and stud were also modelled as contact pairs. The elements on the track flanges and the nodes on the plasterboard were also made as contact pairs. They were in addition to the stud and track contact pairs created for the unlined frames.

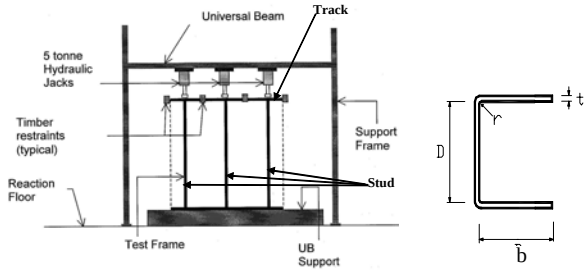

Figure 6. Test Stud Wall Frame

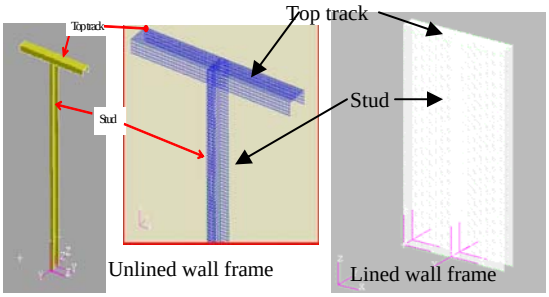

Figure 7. Finite Element Models

Experimentally measured material properties were used for the steel studs and tracks, and the plasterboard. Appropriate local and overall geometric imperfections were included based on the lowest buckling mode obtained from the elastic buckling analyses. Flexural residual stresses were also included in the non-linear analyses. The ultimate loads and the load-displacement curves agree well with experimental results as shown in Table 1 and Figure 8. Figures 9 (a) and (b) show the stress and strain distributions at the ultimate load. The failure mode of the stud from the FEA and experiments can be seen in Figure 9, where the studs failed between the fasteners at the top with the plasterboard exceeding the limit strain of 0.007. This means that pull through of the screws occurred at failure as observed in the full scale tests. The FEA also confirmed the failure mode of flexural torsional buckling between fasteners for 75 mm studs (Figure 9).

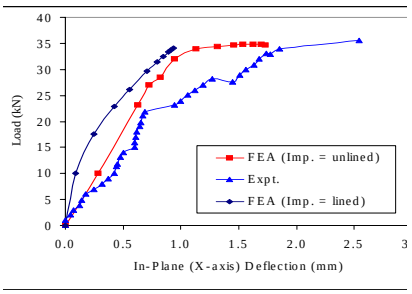

Figure 8. Load-deflection Curve

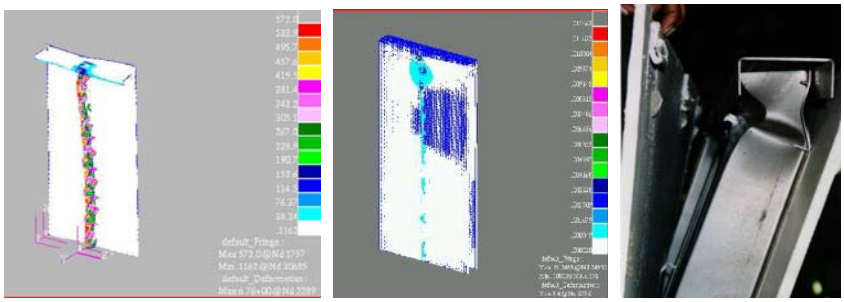

Figure 9. Stress and Strain Distributions in FE Models and Final Failure

3.2 Parametric Study and Design Rules

Parametric studies showed that the ultimate strengths of studs do not depend on the stud spacing and the location of the first screw. The effect of plasterboard thickness can also be ignored as the ultimate loads increased only marginally. However, the ultimate load was influenced by the plasterboard fastener spacing. It was found that the ultimate loads can be estimated by using effective length factors (ELF) based on plasterboard fastener spacing. The ELF about the Y-axis

(K_y) and torsion (K_t) were expressed as the ratio of plasterboard fastener spacing (S_f) to stud length (L) times n (where n = 1, 2, 3,…) and their effects on the ultimate loads were investigated. However, the ELF about the X-axis (K_x) were taken from the design charts for unlined frames [9] as the plasterboard lining did not affect the buckling of studs about X-axis.

The ultimate loads of eight lined wall frames with varying fastener spacing were predicted using various K_y and K_t values. They were computed assuming concentric loading, that is, the load was assumed to be at the effective centroid that takes into account the local buckling effects. By comparing with the ultimate loads from experiments and FEA, it is recommended that the ultimate loads of both sides lined studs walls can be predicted using the following ELF:

- K_x = from the design charts of unlined frames in Figure 10 [9]
- $K_y = K_t = S_f/L$.

The ultimate loads calculated using the above ELF were found to be in good agreement with the FEA and experimental results. However, it was suggested that a factor of 2 shall be applied to the ELF (K_y and K_t) to allow for a defective adjacent screw fastener. AS/NZS 4600 [6] requires that the ultimate strength of the studs under axial compression be computed by (i) ignoring the lining material or (ii) considering the lateral and rotational supports in the plane of the wall. The proposed design method is therefore an improvement to the AS/NZS 4600 method where the lateral and rotational supports in the plane of the wall provided by the lining material have been considered. It has covered both flexural and flexural torsional buckling modes in accordance with AS/NZS 4600 [6] design rules and includes the effective width equations. A similar approach was used for one side lined walls and appropriate design rules were developed [10].

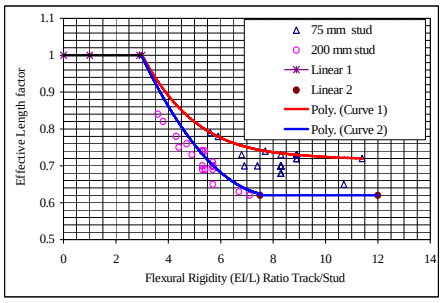

Figure 10. ELF about X-axis

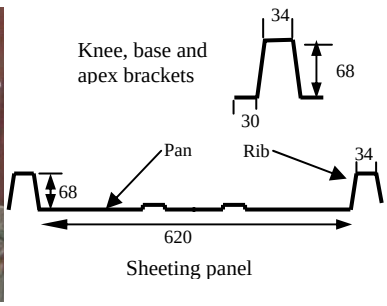

Figure 11. New Cold-formed Steel Building System

4. Cold-formed Steel Building Systems

An Australian shed manufacturer recently developed a new innovative cold-formed steel building system, but detailed research was required to verify its structural adequacy. The new building system has two key differences to that of the conventional portal frame structure. They are that the structure has no conventional frames, and it has no purlins or girts. The structure is essentially fabricated from 0.42 mm G550 steel sheet cladding. However, the key problem is that the load paths and structural behaviour are unknown. Therefore, to determine the adequacy of this structure, full-scale tests and finite element analyses of a 5.4 m x 5.4 m x 2.3 m steel building (10° roof pitch) was conducted under wind uplift and racking loads [11]. Figure 11 shows this innovative 'Frameless' cold-formed steel building. In the frameless structure, the cladding makes up both the roof and wall panels. The ribs of these panels are overlapped to produce the desired length of the structure. The ribbed sections of the structure have twice the thickness of the pans due to overlapping. One bolt in the centre of the ribbed section is used to hold the overlapped ribbed section together. The roof and wall panels are connected together using bolts with 1.5 mm moment resisting brackets at the base, knee and apex (Figure 12).

(a) Base

(b) Knee

Figure 12. Connection Details

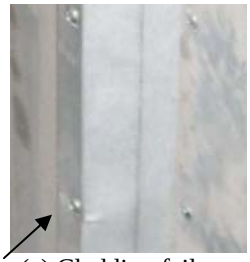

(a) Cladding failure

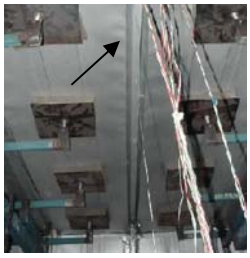

(b) Local buckling of ribs and Pan to rib interface

Figure 13. Cladding Failure and Local Buckling of Ribs

During the non-destructive and destructive full scale tests simulating wind uplift and racking loads, many failures were observed. Load steps of 10% of wind pressure corresponding to a 41 m/s ultimate wind speed was applied until the 140% load level. The first failure occurred at the 50% load level and more failures continued to the 130% load level. By 80% load level the test structure was showing many signs of distress. The most critical one was the cladding failure at the knee brackets at the central three 'frames' (Fig.13). This failure occurred around the lower bolted connection on the rib of the knee brackets. The cladding at this bolted connection buckled inwards with the rotation of the knee brackets. Pans of the panel suffered large deflections while the flanges and webs of the ribs were subjected to local buckling. These failures demonstrate that the cladding thickness of 0.42 mm is not adequate for the required design load (41m/s wind speed).

4.1 Model Description and Validation

Finite element analysis of the new building system was undertaken using ABAQUS 5.8 [4] based on two types of models: strip models and full models. The strip models only model one bay of the building system whereas the full models model the whole building system (Figure 14). The strip model with complex contact conditions is a complex finite element model which models the contact between the overlap of the ribs of the cladding panels and the contact between the bottom cladding panel and the moment resisting brackets. As the brackets, top cladding panels and bottom cladding panels were modelled as separate entities, the nominal thickness of these components were used (0.42 mm for all cladding panels and 1.5 mm for the brackets). Sixty MPC tie elements were used at appropriate locations to simulate the bolted connections which connected the cladding and brackets. To accurately calculate the stress in the high stress areas, a dense mesh (5 mm x 10 mm) of S4R5 shell elements were used for the brackets and the ribs at the ends of the panels. Triangular STRI35 shell elements were used in the transition zone (see insert of Fig.14). To simulate the cast-insitu base brackets of the test structure, fixed base connections were provided. Appropriate symmetric conditions were also used.

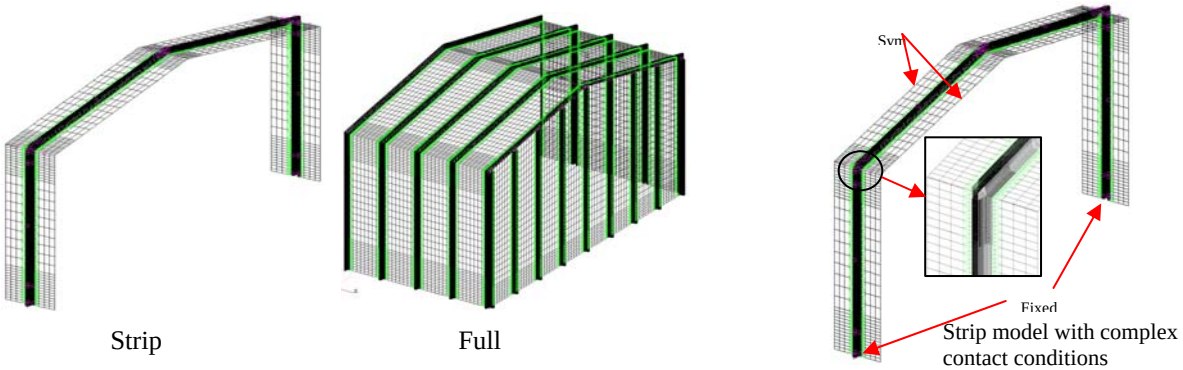

Figure 14. Finite Element Models of Cold-formed Steel Building System

Elastic buckling analyses were also conducted, and the first eigen mode was used to include the initial geometric imperfections in the non-linear analyses. Deflections and stresses agreed reasonably well with test results. Figure 15 compares the local buckling deformation of the cladding panels at the windward knee bracket of the FEA model and the test structure. This local cladding failure was the first failure mode in the experimental test and the FEA model, indicating the ability of FEA model in predicting the failure modes. FE models of the full building system with complex contact conditions were also developed to simulate the diaphragm effects. However, it could not be successfully run due to limitations in computing capacity. Hence the strip model with complex contact conditions was mainly used in this study.

Figure 15. First Failure Mode in FEA and Full Scale Test

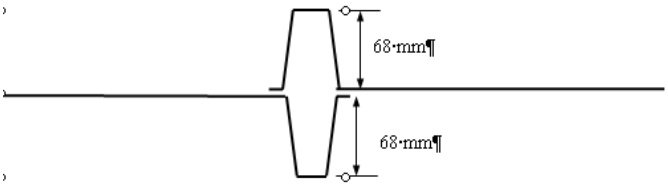

Figure 16. Improved System

4.2 Improvements to Original Building System

To eliminate the failures observed in the building structure and to improve it, FEA were undertaken using the improved strip model. Simplified calculations showed that cladding thickness has to be increased to 0.8 mm. Therefore higher thicknesses were considered in the analyses. However, this will mean almost double the use of steel. Hence modification was also considered by using a more efficient use of the cladding panels. Instead of overlapping the ribbed sections of the cladding panels as adopted in the original building, it was decided to invert every second panel so that the effective depth of the ribbed sections of the cladding panels would be twice that of the original system as seen in Figure 16. The FEA deflections for the destructive cross wind load case with 0.8 mm thickness model and the improved building system are shown in Figure 17, and are compared with the results for the original building (0.42 mm model). Figure 17 shows that the maximum load step achieved for both systems were 2.04 and 2.227 times the design wind load. The original model only reached a load step of 0.84 times the design wind load which correlated well with the first major cladding failure that occurred during the destructive tests. This relates to an increased structural capacity over the original building system of about 143% and 165% for the modified systems. The results also show that the improved system with inverted profile is significantly stiffer than the original building. Both improved systems showed a significant reduction in the extent of local buckling and deflections. In summary, the FEA have shown that an innovative cold-formed building system can be developed to withstand design loads for a wind speed of 41 m/s by either increasing the cladding thickness to 0.8 mm or by using an inverted profile (Fig.16). However, the latter method is recommended since there will not be any increased usage of steel. The new system will have significant economic advantages over portal framed structures.

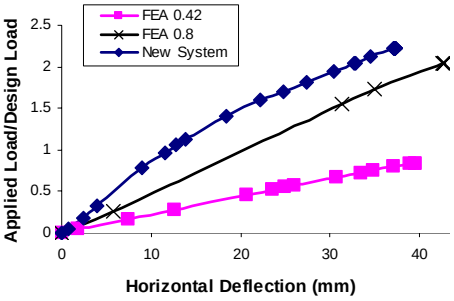

Figure 17. Load-deflection Curves

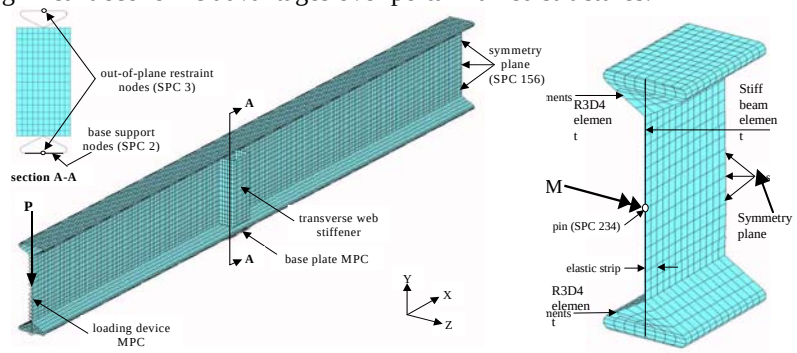

Figure 18. Experimental and Ideal FE Models of HFB

5. Innovative Hollow Flange Beams

An Australian company recently developed a unique cold-formed steel section known as Hollow Flange Beam (HFB) (Fig.18). It is the first cold-formed, hollow flange section to be mass-produced anywhere in the world. The HFB is manufactured from a single strip of high strength steel using a dual process of cold-forming and electric resistance welding. The structural efficiency of the HFB due to the torsionally rigid closed triangular flanges combined with economical fabrication processes was the basis of the HFB development. Since it is a new section and suffers from a relatively new lateral distortional buckling mode when used as flexural members, an investigation [12] was undertaken.

5.1 Model Description and Validation

ABAQUS 5.6 [4] was used for all FEA based on two types of models shown in Fig.18, ie. Experimental model to simulate the experiments with an overhang loading, and Ideal model based on a uniform moment to generate member capacity curves for design purposes. The S4R5 element was selected for HFBs. R3D4 rigid body elements and stiff beam elements were used to create ideal pinned member end restraints for the ideal models. The ABAQUS classical metal plasticity model was used with a simplified bilinear stress-strain curve. Measured values were used in the experimental models while the ideal models incorporated mean measured web and flange yield stresses of 475 and 550 MPa. Idealised boundary conditions as required for flexural members were used except for the experimental model where warping due to the overhang could not be eliminated. The required uniform bending moment was implemented in the ideal models using a moment applied at the section centroid. Single point constraints (SPC) were also applied to the centroidal node to provide a pinned end. Effects of stress concentrations were eliminated by including a 20 mm elastic strip. Appropriate out-of-straightness and twist (global) and local imperfections were modelled in the experimental and ideal models.

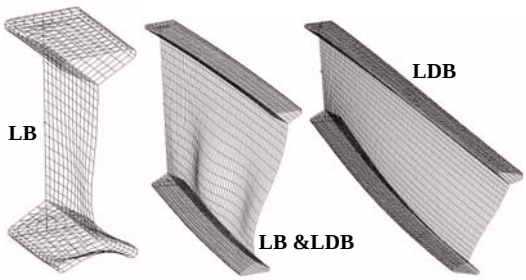

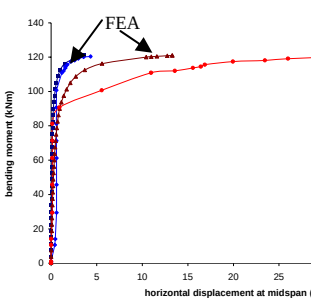

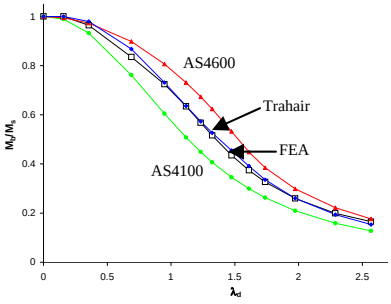

Figure 19. Buckling Modes of HFBs Fig.20. Moment-Displacement Curves Fig.21. Moment Capacity Curves

Elastic buckling analyses were used to obtain the eigenvectors for the geometric imperfection input. Non-linear static analysis was used to obtain the ultimate load capacity. Failure modes of three HFB sections are illustrated in Figure 19. Lateral distortional buckling (LDB) is clearly visible in the 3000 mm span 30090HFB38, flange local buckling (LB) dominates the 500 mm span 25090HFB28, and an interaction between LB and LDB is apparent in the 1500 mm span 45090HFB38. The finite element models were verified by comparison with elastic buckling solutions from THINWALL and with the experimental test results of three HFB sections with spans of 2.4, 3.6 and 4.8 m (Figure 20).

5.2 Parametric Study and Design Rules

The validated ideal non-linear finite element model was used to obtain the moment capacities of the nine HFB sections for a range of spans. The FEA moment capacities were compared with the section *(M_s)* and member *(M_b)* moment capacities obtained from AS4100 and AS/NZS4600 to assess their suitability for HFBs. The AS4100 section and member capacity equations were found to be very conservative while AS/NZS4600 overestimated the member capacity (Fig.21). Therefore a new design procedure was proposed for HFBs based on a modified form of Trahair's equations [13].

$$M_b = \left(b + \frac{a-b}{1+c\lambda_d^{2n}} \right) M_s \le M_s \; ; \quad \text{where non-dimensional member slenderness } \lambda_d = \sqrt{\frac{M_s}{M_{od}}} \qquad (2)$$

The most suitable coefficients (a, b, c and n) were established by solving for the minimum total error for all sections and spans. These values were: a = 1.0, b = 0.0, c = 0.424, and n = 1.196. However, separate coefficients were also obtained for different groups of HFB sections. As seen in Fig.21, the member capacity predicted by the new design procedure is significantly more accurate than the AS4100 and AS4600 predictions. Eq. (2) is therefore recommended for the design of HFB members subject to uniform bending. This HFB section is currently not available in the industry, but other sections have been developed. A similar approach has also been used to develop accurate design procedures for them.

6. Conclusions

This paper has described the extensive use of finite element methods in investigating fully the structural performance of a number of building components and systems. By using four examples of steel cladding systems, innovative hollow flange beams, plasterboard lined cold-formed steel stud walls and an innovative cold-formed steel building system, it has demonstrated the significant benefits of using finite element tools and advanced computing facilities in obtaining safe and optimum building solutions without the need for expensive and time consuming laboratory testing. It has demonstrated how the use of finite element tools has not only allowed the introduction of innovative and efficient building products, but also the development of accurate design methods for use by engineers, manufacturers and designers in the building.

7. Acknowledgements

The author wishes to thank his PhD students (Dr Y. Telue, Dr D. Mahaarachchi, Dr G. Darcy and Dr P. Avery) who undertook the investigations described in this paper as part of their postgraduate studies at QUT.

References

[1] M. Mahendran, *Behaviour and Design of Crest Fixed Profiled Steel Roof Claddings under High Wind Forces*, Eng Struct; Vol.16, No.5, (1994), pp.368-376.

[2] V.R. Beck and L.K. Stevens, *Wind Loading Failures of Corrugated Roof Cladding*, Civil Eng. Trans., IEAust; Vol. 21, No.1, (1979), pp.45-56.

[3] M. Mahendran and R.B. Tang, *Pull-through Strength of High Tensile Steel Cladding Systems*, Australian Journal of Structural Engineering, SE2, (1999), pp.37-49.
[4] Hibbitt, Karlsson and Sorensen (HKS) *ABAQUS User's Manual*, Pawtucket, RI, USA, (1998)
[5] D. Mahaarachchi and M. Mahendran *Finite Element Analysis and Design of Crest-fixed Trapezoidal Steel Claddings with Wide Pans subject to Pull-through Failures*, Engineering Structures, Vol.26, No.11, (2004), pp.1547-1559
[6] Standards Australia (SA), AS/NZS 4600 *Cold-formed Steel Structures*, Sydney, Australia, (1996).
[7] D. Mahaarachchi, *Behaviour and Design of Steel Cladding Systems*, PhD Thesis, QUT, Brisbane, (2003)
[8] Y. Telue and M. Mahendran, *Behaviour of Cold-Formed Steel Wall Frames Lined with Plasterboard*, Journal of Constructional Steel Research, Vol. 57, (2001), pp.435-452.
[9] Y.Telue and M. Mahendran, *Numerical Modelling and Design of Unlined Cold-formed Steel Wall Frames*, J. of Constructional Steel Research, Vol.60, (2003), pp.1241-1256.
[10] Y. Telue and M. Mahendran, *Design of Cold-formed Steel Wall Frames Lined with Plasterboard on One Side under Axial Compression*, International J. of Steel Structures, Vol.6, No.1, (2006), pp.1-12
[11] G. Darcy, *Structural Behaviour of an Innovative Cold-formed Steel Building*, PhD thesis, QUT, Brisbane, (2005).
[12] P. Avery, M. Mahendran and A. Nasir, *Flexural Capacity of Hollow Flange Beams*, J. of Constructional Steel Research, Vol.53, No.2, (2000), pp. 201-223.
[13] N.S. Trahair, *Multiple Design Curves for Beam Lateral Buckling*, Proceedings of the 5th International Colloquium on Stability and Ductility of Steel Structures, Nagoya, Japan, (1997), pp.33-44.